JCTC Journal of Chemical Theory and Computation

Article

pubs.acs.org/JCTC

Quantum Chemical Interpretation of Ultrafast Luminescence Decay and Intersystem Crossings in Rhenium(I) Carbonyl Bipyridine Complexes

Christophe Gourlaouen, Julien Eng, Miho Otsuka, Etienne Gindensperger, and Chantal Daniel*

Laboratoire de Chimie Quantique, Institut de Chimie de Strasbourg UMR-7177 CNRS-UdS, 1 Rue Blaise Pascal BP 296/R8, F-67008 Strasbourg Cedex, France

Supporting Information

ABSTRACT: Ultrafast luminescence decay and intersystem crossing processes through the seven low-lying singlet and triplet excited states of [Re (X)$(CO)_3$(bpy)] (X = Cl, Br, I; bpy = 2,2′-bipyridine) are interpreted on the basis of time-dependent density functional theory (TD-DFT) electronic structure calculations performed in acetonitrile and including spin−orbit coupling (SOC) effects within the zeroth-order approximation. It is shown that the red shift of the lowest part of the spectra by SOC increases from X = Cl (0.06 eV) to X = Br (0.09 eV) and X = I (0.18 eV) due to the participation of the triplet sublevels to the absorption. The six lowest "spin−orbit" states remain largely triplet in character and the maximum of absorption is not drastically affected by SOC. While the energy of the excited states is affected by SOC, the character of these states is not significantly modified: SOC mixes states of the same nature, namely metal-to-ligand-charge-transfer/halide-to-ligand-charge-transfer (MLCT/XLCT). This mixing can be large, however, as illustrated by the S_1/T_2 (a^1A''/a^3A') mixing that amounts to about 50:50 within the series Cl > Br > I. On the basis of the optimized structures of the six lowest excited states an interpretation of the emission signals detected by ultrafast luminescence spectroscopy is proposed. It is shown that whereas the experimental Stokes shift of 6000 cm^{-1} observed for the three complexes is well reproduced without SOC correction for the Cl and Br complexes, SOC effects have to be taken into account for the iodide complex. The early signal of ultrafast luminescence detected immediately after absorption at 400 nm to the S_2 state, covering the 500−550 nm energy domain and characterized by a decay τ_1 = 85 fs (X = Cl) and 128 fs (X = Br), is attributed to S_2 calculated at 505 and 522 nm, respectively, and to some extend to T_3 by SOC. The intermediate band observed at longer time-scale between 550 and 600 nm with emissive decay time τ_2 = 340 fs (X = Cl) and 470 fs (X = Br) can be assigned to T_2 calculated at 558 and 571 nm, respectively. The S_1 state could also participate to this band by SOC. In both complexes the long-lived emission at 600−610 nm is attributed to the lowest T_1 state calculated at 596 and 592 nm for the chloride and bromide complexes, respectively, and shifted to ∼610 nm by SOC. Important SOC effects characterize the luminescence decay of [Re (I)$(CO)_3$(bpy)], the mechanism of which differs significantly of the one proposed for the two other complexes. The A′ spin−orbit sublevel of T_3 state calculated at 512 nm with an oscillator strength of 0.17×10^{-1} participates to the first signal characterized by a rapid decay (τ_1 = 152 fs) with a maximum at 525 nm. The intermediate band covering the 550−600 nm region with a decay time τ_2 = 1180 fs is assigned to the "spin−orbit" S_1 state calculated at 595 nm. The S_2 absorbing state calculated at 577 nm could contribute to these two signals. According to the spin−orbit sublevels calculated for T_1 and T_2, both states contribute to the long-lived emission detected at 600−610 nm, T_1 with two sublevels A′ of significant oscillator strengths of $\sim 10^{-1}$ being the main contributor. In order to follow the evolution of the excited states energy and SOC as a function of the Re−X stretching normal mode their potentials have been calculated without and with SOC as a function of the mass and frequency weighted Re−X stretching mode displacement from the Franck−Condon geometries. Exploratory wavepacket propagations show that SOC alone cannot account for the whole ISC process. Vibronic effects should play an important role in the ultrafast luminescence decay observed experimentally.

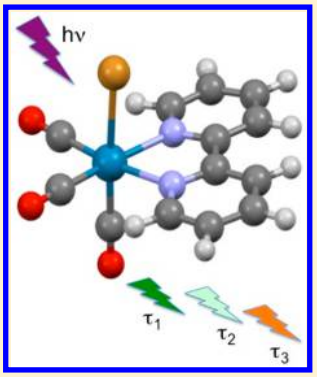

1. INTRODUCTION

The interpretation of ultrafast intersystem crossing (ISC) processes observed in transition metal complexes[1−11] by means of femtosecond luminescence experiments is very challenging for quantum chemistry. It appears that considering spin−orbit coupling (SOC) explicitly is essential to get a correct understanding of these photophysical phenomena. Whereas the use of four-component relativistic approaches is very demanding for electronic excited states calculations in molecules,[12] two component/two-step methods offer a promising option based either on wave function or on density functional theory.[13,14]

Only a few theoretical studies have been dedicated to ISC processes in transition metal complexes. The first detailed investigations of the dynamics of singlet to triplet transitions

Received: September 21, 2014
Published: December 2, 2014

   dx.doi.org/10.1021/ct500846n | J. Chem. Theory Comput. 2015, 11, 99−110

have been performed to understand the photochemical reactivity of HCo $(CO)_4$[15] and HM $(CO)_3(\alpha$-diimine) (M = Mn, Re) molecules,[16−18] that undergo concurrent primary photoreactions whose branching ratio is controlled by ISC from the absorbing state to the reactive states.

More recently, review articles have discussed possible consequences of SOC on the electronic structure, excited state characters, and their deactivation pathways, and demonstrated relations between SOC, the metal-to-ligand-charge-transfer (MLCT) character of the lowest "triplet" state, its zero-field splitting and photoluminescence, that are of paramount importance for OLED applications.[19,20] Spin−orbit calculations of electronic absorption spectra consistently point to large densities of low-lying spin−orbit states and extensive singlet−triplet mixing making void the notion of pure singlet and triplet electronic states.[14,21,22]

Up to now, three types of dynamical simulations, far from being routine, have needed specific developments to be applicable to transition metal complexes and ultrafast phenomena circumscribed by spin-vibronic coupling.

(i) A recent approach, applied to the spin crossover complex $[Fe(bpy)_3]^{2+}$,[10,23,24] is based on time-dependent calculations of ISC rates in the multimode harmonic oscillator and Condon approximations and beyond, where the electronic spin−orbit matrix elements depend linearly on the nuclear coordinates within a spin-vibronic coupling scheme. The ISC rate can be decomposed into three contributions, namely direct, mixed direct vibronic, and vibronic.[25,26]

(ii) The first simulation based on TD-DFT energies and forces (gradient and Hessian) computed on-the-fly and introducing both vibronic and SO coupling effects into the Tully's trajectory surface hopping algorithm has been able to reproduce semiquantitatively the ultrafast relaxation of the photo excited ^{1}MLCT state of $[Ru(bpy)_3]^{2+}$ (bpy = 2,2′-bipyridine) followed by ISC to the lowest ^{3}MLCT state.[27]

(iii) Combined effects of Jahn−Teller (JT) and SOC on the adiabatic PES and electronic spectra of a series of first-row transition metal halides MF_3 (M = Mn, Co, Ti, Cr, and Ni) have been recently investigated from first-principles methods based on the derivation of an Hamiltonian expanded up to linear, quadratic, and higher order in normal modes displacements active for JT distortions and including SOC up to first order in these modes.[28,29] This original work has put in evidence SO induced JT distortions not detectable by the standard model in which SOC is considered as a static property independent of the nuclear motion.

The photophyics of rhenium(I) tricarbonyl complexes $[Re(X)(CO)_3(\alpha$-diimine)] (X = Cl, Br, I), recently investigated by means of ultrafast luminescence spectroscopy,[30] is still the subject of unresolved questions related to SOC. Indeed, two or three ultrafast steps follow optical excitation of their lowest allowed $Re(X)(CO)_3 \rightarrow$ diimine CT transition, the fastest one having been attributed to the $^1CT \rightarrow {}^3CT$ intersystem crossing (ISC). In the halide series, singlet excited-state lifetime counterintuitively increases on going from the chloride (85 fs) to the bromide (128 fs) and iodide (152 fs), whereas SOC between the singlet and triplet states increases in the order Cl < Br ≪ I due to an increase of both the admixture of the halide character to the excited states in question and the halide SOC constant by itself. Moreover, a correlation has been observed between the ISC kinetics and vibrational period of the Re−X stretching mode in similar complexes. In a recent study combining spectroscopic measurements and CASSCF/MS-CASPT2 and TD-DFT calculations, we have shown that whereas both spin-free and spin−orbit quantum chemical calculations simulate UV−vis electronic spectra of $[Re(X)(CO)_3(\alpha$-diimine)] (X = Cl, Br, I) complexes in a reasonable agreement with experiment, they give a very different interpretation of the absorption bands and only the SO treatment can account for the observed spectral features.[14]

The goal of the present study is to go further in our understanding of ultrafast ISC in this class of molecules on the basis of the spin−orbit coupled potential energy curves (PEC) calculated as a function of the Re−X bond stretching mode, for the electronic ground state and the lowest S_1, S_2, S_3, T_1, T_2, T_3, and T_4 excited states of $[Re(X)(CO)_3(bpy)]$ (X = Cl, Br, I; bpy = 2,2′-bipyridine) taking into account solvent effects. The choice of the method has been motivated by the theoretical results of our previous study that has put in evidence the importance of solvent effects in SO-DFT calculations and the limitation of SO-MS-CASPT2 due to restricted active-space size.[14] Moreover the geometries of the lowest six excited states were fully optimized in order to interpret on a static basis the emissive properties of the molecules. Our objective is to provide a comprehensive mechanism of deactivation of the electronic excited states leading to the time-resolved luminescence spectra observed in CH_3CN after irradiation at 400 nm[30] on the basis of a unified picture of the absorption/emission spectroscopy of the three complexes. The computation and analysis of PEC and SOC as a function of the Re−X stretching mode, prior to one-dimensional exploratory wave-packet propagations, should enable us to discuss the measured correlation between the ISC kinetics with the vibrational period of this mode in similar complexes.[30]

2. COMPUTATIONAL DETAILS

The structures of $[Re(X)(CO)_3(bpy)]$ (X = Cl, Br, I) (Figure 1) in the S_0 (a^1A') electronic ground state, the lowest S_1 (a^1A''),

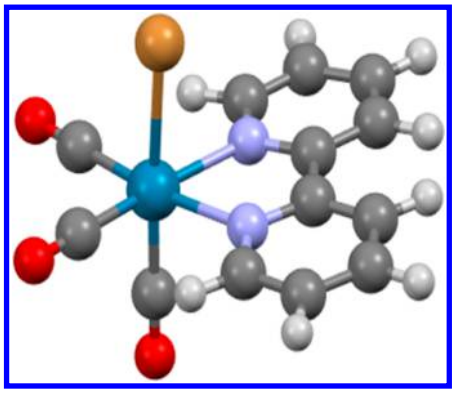

Figure 1. General structure of $[Re(X)(CO)_3(bpy)]$ (**1**: X = Cl; **2**: X = Br; **3**: X = I) complexes.

S_2 (b^1A') and S_3(c^1A') singlet excited states and the T_1 (a^3A''), T_2 (a^3A'), T_3 (b^3A''), and T_4 (b^3A') triplet excited states are optimized under the C_s symmetry constraint at the density functional theory (DFT) level, within the time-dependent approach (TD-DFT) for excited states, using the functional B3LYP[31,32] with all electrons and triple-ζ polarized basis sets.[33]

dx.doi.org/10.1021/ct500846n | J. Chem. Theory Comput. 2015, 11, 99−110

Table 1. TD-DFT Low-Lying Singlet and Triplet States of $[Re(Cl)(CO)_3(bpy)]$ 1, $[Re(Br)(CO)_3(bpy)]$ 2, and $[Re(I)(CO)_3(bpy)]$ 3

	state	assignment	vertical $S_0 \rightarrow S_n$, T_n transition energy (in eV and cm^{-1})	absorption wavelength (in nm)	oscillator strength f
X = Cl **1**					
	T_1 a^3A'' MLCT/XLCT	53% d_{yz} 15% p_z(Cl) $\rightarrow \pi^*_{bpy}$	2.86 (22 880)		
	T_2 a^3A' MLCT/XLCT	49% d_{xy} 17% p_x(Cl) $\rightarrow \pi^*_{bpy}$	2.97 (23 760)		
	S_1 a^1A'' MLCT/XLCT	53% d_{yz} 15% p_z(Cl) $\rightarrow \pi^*_{bpy}$	2.99 (23 920)	418	0.0021
	S_2 b^1A' MLCT/XLCT	49% d_{xy} 17% p_x(Cl) $\rightarrow \pi^*_{bpy}$	3.18 (25 440)	393	0.059
	T_3 b^3A'' IL	81% $\pi_{bpy} \rightarrow \pi^*_{bpy}$	3.23 (25 840)		
	T_4 b^3A' MLCT	63% $d_{Re} \rightarrow \pi^*_{bpy}$	3.34 (26 720)		
	S_3 c^1A' MLCT	98% $d_{Re} \rightarrow \pi^*_{bpy}$	3.38 (27 040)	370	0.0016
X = Br **2**					
	T_1 a^3A'' MLCT/XLCT	47% d_{yz} 25% p_z(Br) $\rightarrow \pi^*_{bpy}$	2.84 (22 720)		
	T_2 a^3A' MLCT/XLCT	42% d_{xy} 28% p_x(Br) $\rightarrow \pi^*_{bpy}$	2.93 (23 440)		
	S_1 a^1A'' MLCT/XLCT	47% d_{yz} 25% p_z(Br) $\rightarrow \pi^*_{bpy}$	2.96 (23 680)	422	0.0017
	S_2 b^1A' MLCT/XLCT	42% d_{xy} 28% p_x(Br) $\rightarrow \pi^*_{bpy}$	3.13 (25 040)	399	0.051
	T_3 b^3A'' IL	81% $\pi_{bpy} \rightarrow \pi^*_{bpy}$	3.22 (25 760)		
	T_4 b^3A' MLCT	63% $d_{Re} \rightarrow \pi^*_{bpy}$	3.34 (26 720)		
	S_3 c^1A' MLCT	98% $d_{Re} \rightarrow \pi^*_{bpy}$	3.37 (26 960)	371	0.0009
X = I **3**					
	T_1 a^3A'' XLCT/MLCT	51% p_z(I) 30% $d_{yz} \rightarrow \pi^*_{bpy}$	2.76 (22 080)		
	T_2 a^3A' XLCT/MLCT	56% p_x(I) 26% $d_{xy} \rightarrow \pi^*_{bpy}$	2.81 (22 480)		
	S_1 a^1A'' XLCT/MLCT	51% p_z(I) 30% $d_{yz} \rightarrow \pi^*_{bpy}$	2.85 (22 800)	438	0.0008
	S_2 b^1A' XLCT/MLCT	56% p_x(I) 26% $d_{xy} \rightarrow \pi^*_{bpy}$	2.95 (23 600)	424	0.029
	T_3 b^3A'' IL/XLCT/MLCT	67% π_{bpy}7% p_z(I)5% $d_{yz} \rightarrow \pi^*_{bpy}$	3.18 (25 440)		
	T_4 b^3A' MLCT	64% $d_{Re} \rightarrow \pi^*_{bpy}$	3.33 (26 640)		
	S_3 c^1A' MLCT	98% $d_{Re} \rightarrow \pi^*_{bpy}$	3.37 (26 960)	371	0.0005

The scalar relativistic effects are taken into account within the zero-order regular approximation (ZORA).[34] The SOC effects are introduced according to a simplified relativistic perturbational TD-DFT formalism.[35,36] The nature of the stationary state was checked through a frequency analysis. The solvent correction is based on the conductor-like screening model (COSMO)[37−39] (with ε = 36.64 for acetonitrile) as implemented in ADF.[40,41]

The "spin-free" (SF) and "spin−orbit" (SO) potential energy curves (PEC) considered for the electronic ground and excited states as a function of the mass and frequency weighted Re−X stretching mode displacements (Q, dimensionless) have been obtained by single point TD-DFT calculations of S_0, S_1, S_2, S_3, T_1, T_2, T_3, and T_4 states, as well as the variation of the SOC along this coordinate. Exploratory wavepacket propagations on the PEC coupled by spin−orbit have been performed for the three complexes using multi configuration time-dependent Hartree (MCTDH) method.[42−44] The SOC variation as a function of the Re−X stretching mode has been taken into account during the propagations.

The calculations have been performed with ADF-2013 quantum chemistry software[45] and the electronic transitions have been analyzed with the Dgrid package.[46]

3. RESULTS AND DISCUSSION

3.1. Electronic Structure. The molecules under investigation are characterized by a d^6 electronic configuration of the rhenium atom and low-lying π^* orbitals localized on the bpy ligand in the electronic ground state. Whereas the HOMO and HOMO−1 of $[Re(Cl)(CO)_3(bpy)]$ and $[Re(Br)(CO)_3(bpy)]$ are composed of about 50% of electronic density localized on the rhenium atom ($5d_{Re}$) and between 15% and 28% of density localized on the halides (p_X, X = Cl, Br), the HOMO−3 is purely localized on the metal and the HOMO−4 is localized on the bpy ligand (π_{bpy}) in both complexes. The LUMO is the π^*_{bpy} antibonding counterpart of the HOMO−4. This electronic structure leads to seven low-lying singlet and triplet-excited states potentially populated upon irradiation at 400 nm (or 25 000 cm^{-1}) (Table 1).

Representative differences of electronic densities corresponding to these $S_0 \rightarrow S_n$, T_n electronic transitions are shown in Figure 2 for illustration. The other densities maps are reported in Supporting Information Figure S1. The results reported in Table 1 show clearly that the chloride and bromide substituted complexes **1** and **2** behave similarly. They are characterized by singlet and triplet states of mixed MLCT/XLCT character with a major contribution of MLCT that decreases when going from Cl to Br.

In contrast the HOMO and HOMO−1 of the iodide complex $[Re(I)(CO)_3(bpy)]$ **3** are composed of more than 50% of p(I) localized contributions with an admixture of about 30% of d_{Re} while the HOMO−3 and HOMO−4 have the same character in the three molecules, namely purely d_{Re} and π_{bpy}, respectively. Consequently, as already pointed out in previous studies the composition of the absorption spectrum of the iodide complex **3** differs significantly from the spectra of the chloride and bromide compounds **1** and **2**.[14,30] The absorption is slightly shifted to the red and the lowest excited states are predominantly XLCT (Table 1) with MLCT contributions never exceeding 30%. Within the domain of energy of interest the three complexes exhibit seven excited states within about

dx.doi.org/10.1021/ct500846n | J. Chem. Theory Comput. 2015, 11, 99−110

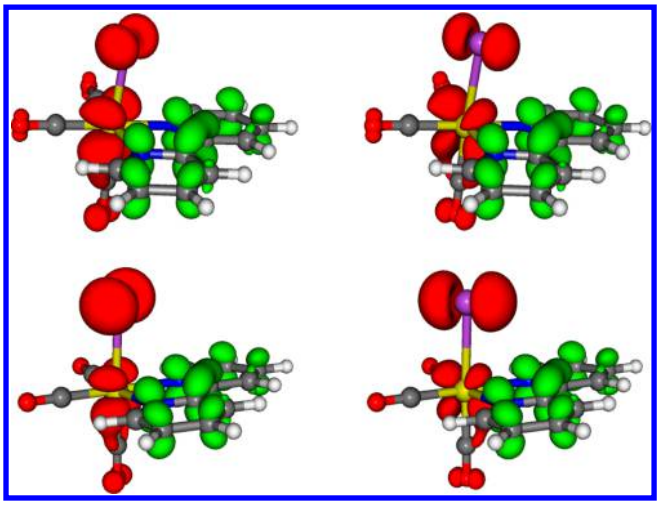

Figure 2. Differences in electronic densities when going from S_0 to S_1/T_1 (top left) and S_2/T_2 (top right) in **2** (X = Br) and from S_0 to S_1/T_1 (bottom left) and S_2/T_2 (bottom right) in **3** (X = I) at the Franck–Condon Geometry. Electronic densities for X = Cl (not shown) are similar to those for Br.

0.5 eV, three singlet's and four triplets, potentially populated either directly upon absorption at 400 nm to S_2 or through singlet–triplet ISC. The absorption wavelengths of S_2 are calculated at 393, 399, and 424 nm for X = Cl, Br, and I, respectively, in good agreement with the experimental spectra recorded in acetonitrile.[14] In order to analyze the role of the triplet states in the ultrafast decay observed after absorption at 400 nm we have calculated the spin–orbit splitting of T_1, T_2, T_3, and T_4 and the SOC between the seven excited states reported in Table 1. The SOC effects are reported in Table 2 for the three complexes.

When SOC is included the seven "spin-free" excited states described in Table 1 generate 15 "spin–orbit" states in the relevant domain of energy of the spectra of [Re(Cl)-$(CO)_3$(bpy)], [Re(Br)$(CO)_3$(bpy)] and [Re(I)$(CO)_3$(bpy)]. The results reported in Table 2 compare well to the data we have published earlier on the same systems but using different solvent and various functionals and methods.[14] The "spin–orbit" spectra of the three molecules that agree rather well with the experimental spectra recorded in CH_3CN are depicted in Supporting Information Figure S2. Within the present zeroth-order approximation the SOC perturbation has already several effects on the absorption spectroscopy of the complexes:

(i) The lowest part of the spectra is red-shifted by 0.06 eV (X = Cl), 0.09 eV (X = Br) and 0.18 eV (X = I) due to the participation of the triplet sublevels to the absorption;

(ii) The six lowest "spin–orbit" states remain largely "triplet" in character, the only significant singlet contributions being present in E_3/E_4 (X = Cl: 46% in E_4), (X = Br: 10% in E_3; 44% E_4) and (X = I: 44% in E_3; 26% in E_4);

(iii) The maximum of absorption originated from the S_2 (b^1A') state is not drastically affected by the SOC corrections, the only alterations being a decrease of the oscillator strength by mixing with the IL b^3A'' state (X = Cl, Br) or the XLCT/MLCT a^3A'' state (X = I) and a small blue shift (160 cm^{-1}) of the maximum in the iodide complex **3**;

(iv) The character of the lowest states below S_2, namely MLCT/XLCT for the chloride and bromide complexes and XLCT/MLCT for the iodide complex, is not modified by SOC interactions;

(v) The SOC splitting of the triplet states never exceeds 0.06 eV (480 cm^{-1}) leading to several sets of nearly degenerate electronic states of moderate to weak intensities.

As illustrated by the results reported in Table 2 the singlet–triplet mixing by SOC can become important and does not follow the heavy-atom rules. For instance the S_1/T_2 (a^1A''/a^3A') mixing amounts to about 50:50 within the series Cl > Br > I. Here the predominant MLCT character of these states in the chloride and bromide complexes may compensate the larger SOC effect in the iodide compound.

In order to interpret the luminescence properties of the three complexes the structures of the six low-lying singlet and triplet states, namely S_1, S_2, T_1, T_2, T_3, and T_4, have been optimized at the same level of calculation than the one of the electronic ground state. The geometries of the "spin-free" states described in this section (Table 1) have been optimized. Their energy has been corrected a posteriori by SOC perturbation. The structural properties and emissive properties of these excited states are discussed in the two next sections.

3.2. Structural Properties. Some important structural parameters extracted from the optimized geometries of complexes [Re(Cl)$(CO)_3$(bpy)] **1**, [Re(Br)$(CO)_3$(bpy)] **2**, and [Re(I)$(CO)_3$(bpy)] **3** in the electronic ground state and low-lying triplet and singlet excited states are reported in Table 3. The S_1 and T_1 geometries converged to a C_s solution, validated by a frequency analysis. However, the Cs symmetry has been retained during the optimization procedure for S_2 and T_2 states to avoid convergence problems. A single imaginary frequency (<100 cm^{-1}) remains in the C_s structures.

The structural deformations when going from the electronic ground state to the relaxed low-lying singlet and triplet exited states are quite small. After nuclear relaxation into the potential wells of the excited states S_1, S_2, T_1, T_2, and T_3 the Re–X shortening does not exceed 0.097 Å in the singlet states and 0.043 Å in the triplet states. This deformation is accompanied by an elongation of the Re–C_{ax} bonds (<3%) together with a minor shortening of the Re–N bonds in all excited states. In contrast to the MLCT/XLCT, XLCT/MLCT and IL states, the pure MLCT state T_4 is characterized by a small elongation of the Re–X bond in the bromide and iodide substituted complexes. The T_1 and T_2 triplet states in the bromide and iodide substituted complexes are the seat of a moderate bending of the XRe–C_{ax} angle complemented by an opening of the NReX angle. This effect increases with the XLCT character and is especially significant in the T_2 states where the XReC_{ax} angle decreases from 178.9° to 169° and from 177.9° to 164.1° in [Re(Br)$(CO)_3$(bpy)] and [Re(I)$(CO)_3$(bpy)], respectively. As illustrated in Table 3 the other important geometrical parameters are not drastically modified when going from the electronic ground state to the excited states whatever the halide ligand is.

In the next section, the above structural data are used to provide a qualitative interpretation of the emissive properties of the three molecules.

3.3. Emission Properties. The energy of the relaxed lowest excited states S_1, S_2, T_1, T_2, T_3, and T_4 under C_s symmetry constraint and corrected by SOC perturbation at their "spin-free" optimized geometries are summarized in Table 4 for the three complexes.

dx.doi.org/10.1021/ct500846n | J. Chem. Theory Comput. 2015, 11, 99–110

Table 2. Spin−Orbit Coupled Low-Lying Excited States of $[Re(Cl)(CO)_3(bpy)]$ 1, $[Re(Br)(CO)_3(bpy)]$ 2, and $[Re(I)(CO)_3(bpy)]$ 3 Calculated at the TD-DFT Level

	state	composition	vertical $S_0 \rightarrow E_n$ transition energy (in eV and cm^{-1})	oscillator strength f
X = Cl **1**				
	E_1 (A″) MLCT/XLCT	71% a^3A'' 24% a^3A'	2.78 (22 240)	2.0×10^{-6}
	E_2 (A′) MLCT/XLCT	72% a^3A'' 24% a^3A'	2.78 (22 240)	0.99×10^{-4}
	E_3 (A′) MLCT/XLCT	88% a^3A'	2.81 (22 480)	0.004
	E_4 (A″) MLCT/XLCT	48% a^3A'46% a^1A''	2.85 (22 800)	0.95×10^{-3}
	E_5 (A″) MLCT/XLCT	72% a^3A' 26% a^3A''	3.01 (24 080)	0.68×10^{-3}
	E_6 (A′) MLCT/XLCT	72% a^3A' 26% a^3A''	3.01 (24 080)	0.10×10^{-3}
	E_7 (A″) MLCT/XLCT	50% a^3A' 49% a^1A''	3.07 (24 560)	0.24×10^{-5}
	E_8 (A′) MLCT/IL/XLCT	58% b^1A' 26% b^3A''	3.17 (25 360)	0.035
	E_9 (A″) IL	94% b^3A''	3.23 (25 840)	0.39×10^{-6}
	E_{10} (A′) IL	95% b^3A''	3.23 (25 840)	0.82×10^{-4}
	E_{11} (A′) IL/MLCT/XLCT	72% b^3A'' 26% b^1A'	3.25 (26 000)	0.016
	E_{12} (A″) MLCT	92% b^3A'	3.37 (26 960)	0.43×10^{-5}
	E_{13} (A″) MLCT	92% b^3A'	3.37 (26 960)	0.12×10^{-3}
	E_{14} (A′) MLCT	87% b^3A'	3.38 (27 040)	0.47×10^{-2}
	E_{15} (A′) MLCT	93% c^1A'	3.41 (27 280)	0.15×10^{-2}
X = Br **2**				
	E_1 (A″) MLCT/XLCT	66% a^3A'' 30% a^3A'	2.75 (22 000)	0.21×10^{-5}
	E_2 (A′) MLCT/XLCT	66% a^3A'' 30% a^3A'	2.75 (22 000)	0.51×10^{-4}
	E_3 (A′) MLCT/XLCT	86% a^3A'' 10% b^1A'	2.78 (22 240)	0.52×10^{-2}
	E_4 (A″) MLCT/XLCT	44% a^1A'' 50% a^3A'	2.80 (22 400)	0.74×10^{-3}
	E_5 (A″) MLCT/XLCT	66% a^3A' 31% a^3A''	2.99 (23 920)	0.58×10^{-5}
	E_6 (A′) MLCT/XLCT	66% a^3A' 31% a^3A''	2.99 (23 920)	0.93×10^{-4}
	E_7 (A″) MLCT/XLCT	51% a^1A'' 48% a^3A'	3.05 (24 400)	0.86×10^{-3}
	E_8 (A′) MLCT/XLCT/IL	70% b^1A' 14% b^3A''	3.13 (25 040)	0.036
	E_9 (A″) IL	95% b^3A''	3.22 (25 760)	0.12×10^{-5}
	E_{10} (A′) IL	96% b^3A''	3.22 (25 760)	0.88×10^{-4}
	E_{11} (A′) IL/MLCT/XLCT	82% b^3A'' 16% b^1A'	3.23 (25 840)	0.80×10^{-2}
	E_{12} (A″) MLCT	92% b^3A'	3.35 (26 800)	0.35×10^{-5}
	E_{13} (A′) MLCT	92% b^3A'	3.36 (26 880)	0.20×10^{-3}
	E_{14} (A′) MLCT	91% b^3A'	3.36 (26 880)	0.16×10^{-2}
	E_{15} (A′) MLCT	94% c^1A'	3.39 (27 120)	0.85×10^{-3}
X = I **3**				
	E_1 (A″)XLCT/MLCT	55% a^3A'' 42% a^3A'	2.58 (20 640)	0.14×10^{-5}
	E_2 (A′) XLCT/MLCT	54% a^3A'' 42% a^3A'	2.58 (20 640)	0.14×10^{-4}
	E_3 (A″) XLCT/MLCT	54% a^3A' 44% a^1A''	2.62 (20 960)	0.34×10^{-3}
	E_4 (A′) XLCT/MLCT	70% a^3A'' 26% b^1A'	2.62 (20 960)	0.76×10^{-2}
	E_5 (A″) XLCT/MLCT	52% a^3A' 40% a^3A''	2.88 (23 040)	0.10×10^{-5}
	E_6 (A′) XLCT/MLCT	51% a^3A' 40% a^3A''	2.90 (23 200)	0.18×10^{-2}
	E_7 (A″) XLCT/MLCT	49% a^1A'' 42% a^3A'	2.93 (23 440)	0.38×10^{-3}
	E_8 (A′) XLCT/MLCT	62% b^1A' 24% a^3A''	2.97 (23 760)	0.018
	E_9 (A″) IL/XLCT/MLCT	89% b^3A''	3.17 (25 360)	0.44×10^{-5}
	E_{10} (A′) IL/XLCT/MLCT	88% b^3A''	3.17 (25 360)	0.13×10^{-3}
	E_{11} (A′) IL/XLCT/MLCT	94% b^3A''	3.18 (25 440)	0.16×10^{-2}
	E_{12} (A″) MLCT/XLCT	64% b^3A' 24% a^3A'	3.28 (26 240)	0.30×10^{-4}
	E_{13} (A″) MLCT	62% b^3A'	3.28 (26 240)	0.34×10^{-4}
	E_{14} (A′) MLCT	75% b^3A'	3.31 (26 480)	0.31×10^{-2}
	E_{15} (A′) MLCT	39% c^1A' 30% c^3A'	3.46 (27 680)	0.70×10^{-3}

According to the calculations the luminescence should start from the S_2 state at 505 and 522 nm for the chloride and bromide complexes, giving Stokes shifts of 5640 and 5880 cm^{-1}, respectively, in agreement with the exprimental data (~6000 cm^{-1}). Accordingly, the two complexes behave similarly and the small calculated red-shift is also observed on the experimental luminescence spectra when going from Cl to Br.[30] On the basis of the results without SOC reported in Table 4 a qualitative interpretation of the time-resolved luminescence of $[Re(Cl)(CO)_3(bpy)]$ and $[Re(Br)(CO)_3(bpy)]$ spectra is proposed:

The early signal detected immediately after absorption at 400 nm, covering the 500−550 nm energy domain and characterized by a rapid decay, τ_1 = 85 fs (X = Cl) and 128 fs (X = Br), is attributed to the S_2 state in both complexes. The T_3 state could also contribute to this emission by SOC with a maximum calculated at 482 nm and a significant oscillator strength $f = 0.24 \times 10^{-1}$. The intermediate band observed at longer timescale between 550 and 600 nm with emissive decay time τ_2 =

dx.doi.org/10.1021/ct500846n | J. Chem. Theory Comput. 2015, 11, 99−110

Table 3. Optimized Representative Bond Lengths (in Å) and Bond Angles (in Degree) of [Re(Cl)(CO)$_3$(bpy)] 1, [Re(Br)(CO)$_3$(bpy)] 2, and [Re(I)(CO)$_3$(bpy)] 3 in the S_0 Electronic Ground State and Low-Lying S_1, S_2 Singlet and T_1, T_2, T_3, T_4 Triplet States Calculated in CH_3CN

	S_0	S_1	S_2	T_1	T_2	T_3	T_4
X = Cl **1**		MLCT/XLCT	MLCT/XLCT	MLCT/XLCT	MLCT/XLCT	IL	MLCT
Re−X	2.552	2.455	2.473	2.480	2.509	2.512	2.550
Re−N	2.204	2.165	2.187	2.149	2.157	2.194	2.154
Re−C_{ax}	1.907	1.968	1.946	1.961	1.939	1.928	1.914
Re−C_{eq}	1.925	1.955	1.952	1.956	1.959	1.936	1.988
C−C_{bpy}	1.472	1.415	1.426	1.411	1.421	1.396	1.418
NReN	74.1	76.2	76.0	76.6	76.0	74.4	75.9
$C_{eq}ReC_{eq}$	88.3	83.6	95.6	84.2	94.9	86.8	89.6
$XReC_{ax}$	178.0	173.4	179.0	174.1	173.3	175.1	172.3
NReX	84.1	86.4	88.2	86.7	89.8	84.2	84.1
X = Br **2**		MLCT/XLCT	MLCT/XLCT	MLCT/XLCT	MLCT/XLCT	IL	MLCT
Re−X	2.713	2.616	2.654	2.646	2.693	2.678	2.727
Re−N	2.204	2.166	2.181	2.150	2.158	2.195	2.153
Re−C_{ax}	1.907	1.965	1.936	1.958	1.930	1.934	1.912
Re−C_{eq}	1.925	1.953	1.953	1.954	1.958	1.934	1.989
C−C_{bpy}	1.471	1.415	1.426	1.411	1.422	1.397	1.418
NReN	74.0	76.1	76.0	76.6	76.1	74.4	75.8
$C_{eq}ReC_{eq}$	88.3	84.0	95.7	84.5	94.6	87.2	89.4
$XReC_{ax}$	178.9	174.5	173.9	175.3	169.0	175.8	174.3
NReX	85.0	87.9	91.6	88.2	92.9	85.2	85.8
X = I **3**		XLCT/MLCT	XLCT/MLCT	XLCT/MLCT	XLCT/MLCT	IL/XLCT/MLCT	MLCT
Re−X	2.911	2.823	2.879	2.846	2.942	2.914	2.949
Re−N	2.205	2.173	2.186	2.158	2.157	2.198	2.156
Re−C_{ax}	1.909	1.959	1.928	1.957	1.919	1.914	1.912
Re−C_{eq}	1.925	1.948	1.947	1.950	1.954	1.929	1.986
C−C_{bpy}	1.470	1.416	1.425	1.412	1.422	1.396	1.417
NReN	74.0	75.9	75.8	76.3	76.1	74.3	75.4
$C_{eq}ReC_{eq}$	88.6	85.0	95.0	85.1	94.1	88.3	91.2
$XReC_{ax}$	177.9	176.3	170.8	176.9	164.1	176.7	176.5
NReX	86.0	89.1	93.9	89.4	95.0	85.1	87.1

340 fs (X = Cl) and 470 fs (X = Br) can be assigned to the T_2 state calculated at 558 nm (X = Cl) and 571 nm (X = Br). By SOC this triplet state gains oscillator strength (0.2×10^{-3}) and becomes coupled to the S_1 state (see Table 2). To some extent the S_1 state calculated at ∼550 nm ($f = 0.2 \times 10^{-2}$) (stabilized at ∼570 nm by SOC), despite of it's A″ symmetry, should participate indirectly to this intermediate band. In both molecules, the observed long-lived emission at 600−610 nm is attributed to the lowest T_1 states calculated at 596 and 592 nm for the chloride and bromide complexes, respectively, and shifted to ∼610 nm with $f = 0.6 \times 10^{-2}$ by SOC in better agreement with experimental data.

As shown in Table 4, the SOC effects are not dramatic and can be neglected as far as the emissive properties of [Re(Cl)(CO)$_3$(bpy)] and [Re(Br)(CO)$_3$(bpy)] are concerned. Indeed, the SOC induced splitting of the lowest emissive triplet states is very small. The good agreement between experimental and theoretical Stokes shifts (about 6000 cm^{-1}) obtained for the Cl and Br substituted complexes without SOC correction confirms this assumption. Moreover, the reasonable qualitative correlation between the calculated minima of the emissive states and the energy domain of the observed luminescence time-resolved signals corroborate our interpretation. However, the SOC will be important for describing the nonadiabatic dynamics of the excited states coupled vibronically as well as by spin−orbit.[29]

In contrast, the results reported in Table 4 for [Re(I)(CO)$_3$(bpy)] indicate important SOC effects on the emissive properties of the iodide complex. The Stokes shift calculated from S_2 emission without SOC (4944 cm^{-1}) is underestimated as compared to the value obtained with SOC, namely 6430 cm^{-1} closer to the experimental data.[30] When analyzing the SOC corrected results reported in Table 4 for [Re(I)(CO)$_3$(bpy)] a qualitative interpretation of the time-resolved luminescence spectrum can be given:

The first signal characterized by a rapid decay (τ_1 = 152 fs) and a maximum at 525 nm is attributed to the "spin−orbit" A′ component of the T_3 state calculated at 512 nm with $f = 0.17 \times 10^{-1}$ and to the S2 state calculated at 577 nm with $f = 0.4 \times 10^{-1}$. The intermediate band covering the 550−600 nm region with a decay time τ_2 = 1180 fs is assigned to the "spin−orbit" S_1 state calculated at 595 nm. The S_2 state could also contribute to this intermediate band. According to the values obtained for the spin−orbit sublevels of the T_1 and T_2 states (Table 4) both states should contribute to the observed long-lived emission detected at 600−610 nm. However, T_1 that acquires significant oscillator strength by SOC ($f = 0.15 \times 10^{-1}$) is probably the main contributor to the long-lived luminescence.

Scheme 1 gives a qualitative picture of the luminescence decay through the low-lying singlet and triplet states of the three complexes on the basis of emission wavelengths collected in Table 4, namely without SOC for chloride and bromide

dx.doi.org/10.1021/ct500846n | J. Chem. Theory Comput. 2015, 11, 99−110

Table 4. TD-DFT Vertical S_n, $T_n \rightarrow S_0$ Transition Energies (in eV) and Corresponding Emission Wavelengths (in nm) of the Lowest Relaxed Singlet and Triplet States of $[Re(Cl)(CO)_3(bpy)]$ 1, $[Re(Br)(CO)_3(bpy)]$ 2, and $[Re(I)(CO)_3(bpy)]$ 3 Calculated in CH_3CN

	state	vertical S_n, $T_n \rightarrow S_0$ transition energy (in eV)	emission wavelength (in nm)	emission wavelength (in nm) with SOC
X = Cl **1**				
	T_1 (a^3A'')	2.096	596	610 (A″)
				610 (A′)
				607 (A′)
	T_2 (a_3A')	2.239	558	575 (A″)
				576 (A′)
				570 (A″)
	S_1 (a^1A'')	2.245	557	575 (A″)
	S_2 (b^1A')	2.474	505	496 (A′)
	T_3 (b^3A'')	2.637	474	482 (A′)
				472 (A″)
				466 (A″)
	T_4 (b^3A')	2.724	459	453 (A″)
				451 (A″)
				449 (A′)
X = Br **2**				
	T_1 (a^3A'')	2.113	592	609 (A″)
				608 (A′)
				604 (A′)
	T_2 (a^3A')	2.1894	571	587 (A″)
				587 (A′)
				583 (A″)
	S_1 (a^1A'')	2.260	553	576 (A″)
	S_2 (b^1A')	2.393	522	505 (A′)
	T_3 (b^3A'')	2.623	477	487 (A′)
				467 (A″)
				467 (A′)
	T_4 (b^3A')	2.722	459	454 (A″)
				452 (A″)
				447 (A′)
X = I **3**				
	T_1 (a^3A'')	2.129	587	620 (A″)
				619 (A′)
				612 (A′)
	T_2 (a^3A')	2.096	596	620 (A″)
				620 (A′)
				617 (A″)
	S_1 (a^1A'')	2.263	552	595 (A″)
	S_2 (b^1A')	2.331	536	577 (A′)
	T_3 (b^3A'')	2.539	492	512 (A′)
				483 (A′)
				479 (A″)
	T_4 (b^3A')	2.725	459	459 (A″)
				458 (A′)
				458 (A″)

substituted complexes **1** and **2** and with SOC perturbation for complex **3**.

On the basis of the static electronic and structural properties of the three complexes discussed in this section, we cannot get time scales associated with the time-resolved luminescence spectra.[30] In order to study the population of the active excited states in real time as a function of the nuclear relaxation, it is necessary to perform nonadiabatic quantum dynamics within a multimode approach applied to spin-vibronically coupled excited states. This type of simulation is very challenging for transition metal complexes[28,29,47] and is beyond the scope of the present paper. Instead, we propose here exploratory wavepacket propagations on the spin−orbit coupled PEC associated with the singlet and triplet excited states discussed above and calculated as a function of the mass and frequency weighted Re−X stretching mode. This simulation is the first step toward the analysis of the experimental evidence of a correlation between the ISC times measured for the $[Re(X)(CO)_3(bpy)]$ complexes and the vibrational period of the Re−X stretching mode in similar complexes.[30] The PEC calculated without and with SOC are presented in the next section together with the variation of the SOC as a function of this coordinate for the three complexes.

3.4. Potential Energy Curves. The gradients analysis shows an important contribution of the Re−X stretching mode around the FC region, especially for S_2 and S_1 states. This will have important consequences at the early stage of the photophysical process. A frequency analysis of the normal modes in the S_0 electronic ground state within the harmonic approximation and corrected by solvent effects has been performed for the three complexes. In each case, a stretch frequency is identified at 236, 152, and 125 cm^{-1} for $[Re(Cl)(CO)_3(bpy)]$ **1**, $Re(Br)(CO)_3(bpy)]$ **2**, and $[Re(I)(CO)_3(bpy)]$ **3**, respectively. This mode is associated with a deformation of the bpy ligand corresponding to an out-of-plane bending mode for **3** and an in-plane scissoring mode for **1** and **2** (Figure 3).

The TD-DFT and SOC corrected TD-DFT potential energy curves calculated as a function of the mass and frequency weighted Re−X stretching mode displacements (Q, dimensionless) and associated with S_1, S_2, S_3, T_1, T_2, T_3, and T_4 excited states described in Table 1 are depicted in Figure 4 for $[Re(Br)(CO)_3(bpy)]$ and in Supporting Information Figures S3 and S4 for $[Re(Cl)(CO)_3(bpy)]$ and $[Re(I)(CO)_3(bpy)]$, respectively.

The minima of the excited states are shifted to shorter Re−Br distances as compared to the FC point (Table 3) with values varying between 2.56 and 2.61 Å. The T_1 and T_2 states remain the lowest states along this coordinate and the degeneracy between the S_1 and T_2 states is left at long distances. The T_3 and T_4 states present a crossing point at long Re−Br distances that should not take part into the ultrafast decay mechanism. When SOC is applied (Figure 4 bottom) 15 potential energy curves are generated corresponding to the E_n states described in Table 2. T_1 and T_2 lead to two sets of degenerated E_1/E_2 and E_5/E_6 potentials, whereas E_3 is essentially composed of T_1. The singlet components are minor in these "spin−orbit" potentials. In contrast the E_4 and E_7 potentials correspond to a 50:50 S_1/T_2 mixing whereas E_8 and E_{11} are generated by S_2/T_1 mixing with a major contribution of S_2 in E_8 that remains the absorbing state with a minimum at short Re−Br bond distance (2.60 Å). The upper T_3 and T_4 states give rise to two sets of three nearly degenerate potentials at FC that interact nonadiabatically at longer distances as illustrated by the presence of avoided crossings in Figure 4. The S_3 potential remains nearly purely singlet (E_{15}) and does not cross the upper E_n triplet potentials. The lowest "spin−orbit" states of interest run more or less in a parallel way with no crossings around the FC region along this A′ normal mode of vibration.

The PEC associated with the low-lying excited states of $[Re(Cl)(CO)_3(bpy)]$ **1** and $[Re(I)(CO)_3(bpy)]$ **3** are

dx.doi.org/10.1021/ct500846n | J. Chem. Theory Comput. 2015, 11, 99−110

Scheme 1. Qualitative Representation of the Mechanism of Luminescent Decay of (a) [Re(Cl)(CO)$_3$(bpy)] 1, [Re(Br)(CO)$_3$(bpy)] 2, and (b) [Re(I)(CO)$_3$(bpy)] 3 after Absorption to S$_2$ at 400 nm[a]

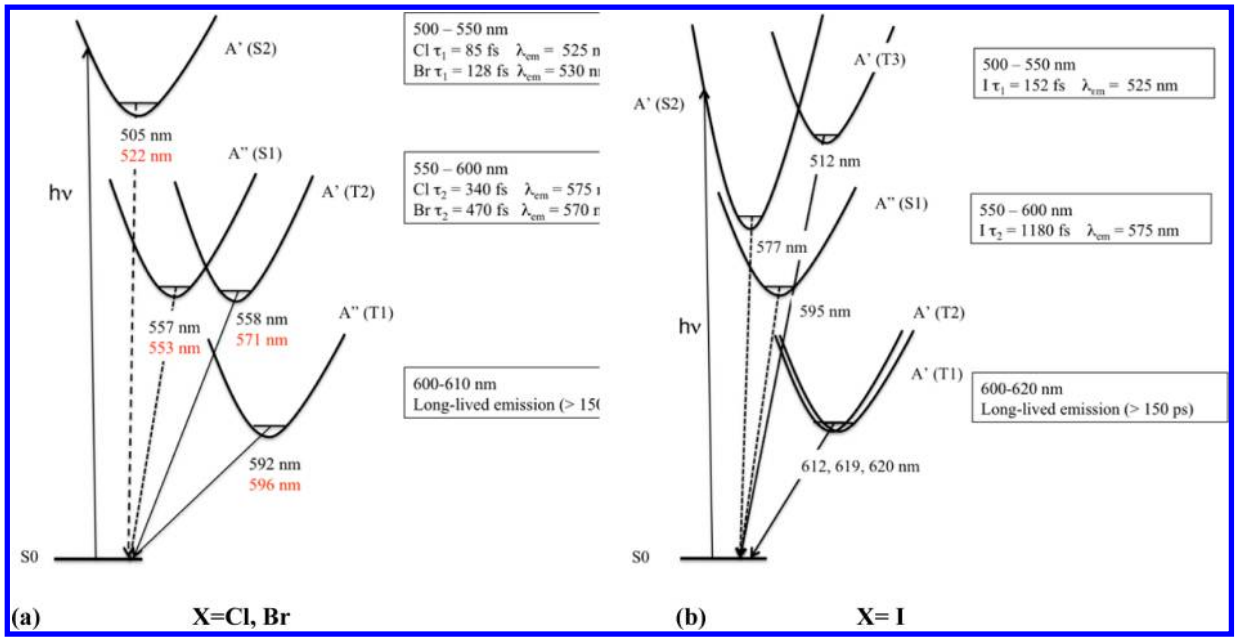

[a]The calculated emission wavelengths (in nm) are reported in black (X = Cl) and red (X = Br). The experimental data from ref 30 are reported on the right of the diagrams for comparison.

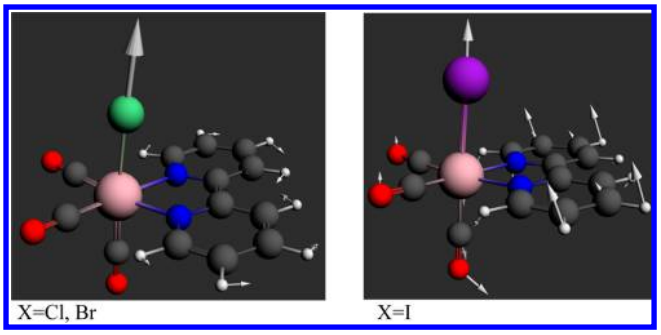

Figure 3. Representation of the Re−X stretching mode displacements in the S$_0$ electronic ground state of [Re(Cl)(CO)$_3$(bpy)] **1**, [Re(Br)(CO)$_3$(bpy)] **2**, and [Re(I)(CO)$_3$(bpy)] **3** in CH_3CN.

represented in Supporting Information Figures S3 and S4, respectively. Whereas only "spin-free" potentials of the chloride, bromide and iodide complexes show comparable characteristics, both "spin−orbit" and "spin-free" potentials of **1** and **2** are similar. This corroborates the common luminescent decay behavior of the two complexes upon irradiation at 400 nm and the absence of heavy atom effect into the ultrafast process when replacing Cl by Br. The "spin−orbit" potentials of the iodide complex **3** differ significantly of the others. Indeed, they are characterized by the occurrence of a number of avoided crossings when elongating the Re−I bond above 23 000 cm^{-1}. Moreover five sets of degenerate potentials coexist, namely E$_1$/E$_2$, E$_3$/E$_4$, E$_5$/E$_6$, E$_7$/E$_8$, and E$_9$/E$_{10}$ potentially populated upon irradiation at 400 nm, either directly or by spin-vibronic coupling. This picture confirms the participation of both lowest triplet states T$_1$ and T$_2$, more precisely their SOC sublevels E$_1$/E$_2$ and E$_3$/E$_4$, to the long-lived emission of [Re(I)(CO)$_3$(bpy)] as deduced from the emission properties discussed in section 3.3.

Whereas E$_8$ generated by S$_2$ remains the only absorbing state in the chloride and bromide complexes, four "spin−orbit" states, namely E$_5$/E$_6$ and E$_7$/E$_8$ and to lesser extent E$_9$/E$_{10}$/E$_{11}$ may participate to the absorption of [Re(I)(CO)$_3$(bpy)]. Similarly these two sets of sublevels generated by SOC will contribute to the 2-fold luminescence decay observed at the early time below 1 ps.[30]

The variations of SOC between the singlet and triplet electronic states calculated as a function of the Re−X stretching normal mode are represented in Figure 5 for [Re(Br)(CO)$_3$(bpy)] **2** and in Supporting Information Figures S5 and S6 for [Re(Cl)(CO)$_3$(bpy)] **1** and [Re(I)(CO)$_3$(bpy)] **3**, respectively.

The real and imaginary parts of the SOC are equally important but act differently on the calculated singlet/triplet and triplet/triplet SOC as a function of the Re−Br stretching mode. At short Re−Br distances, especially around FC, the S$_1$/T$_2$ and S$_2$/T$_1$ SOC (real contribution) are greater than 500 cm^{-1} (Figure 5 top) and remain nearly constant. In contrast, their imaginary contributions is rather small with values of ∼150 cm^{-1} (Figure 5 bottom). The T$_1$/T$_2$ interaction follows the same trends. The SOC between S$_1$, S$_2$ and the upper T$_3$ and T$_4$ triplet states does not exceed 200 cm^{-1} as far as the real part is concerned but may reach 600 cm^{-1} when imaginary contribution is considered. Globally, we may distinguish between two sets of SOC, namely a series below 200 cm^{-1} and a second one above 500 cm^{-1}. These values are not really affected by the Re−Br bond stretching mode since the character of the excited states is not strongly modified along this coordinate. The same behavior characterizes the chloride complex **1** (Supporting Information Figure S5). Again the heavy-atom effect along the halide series does not play an important role since on one hand Br is heavier than Cl but the low-lying excited states of the chloride complex have a slightly more pronounced metal character.

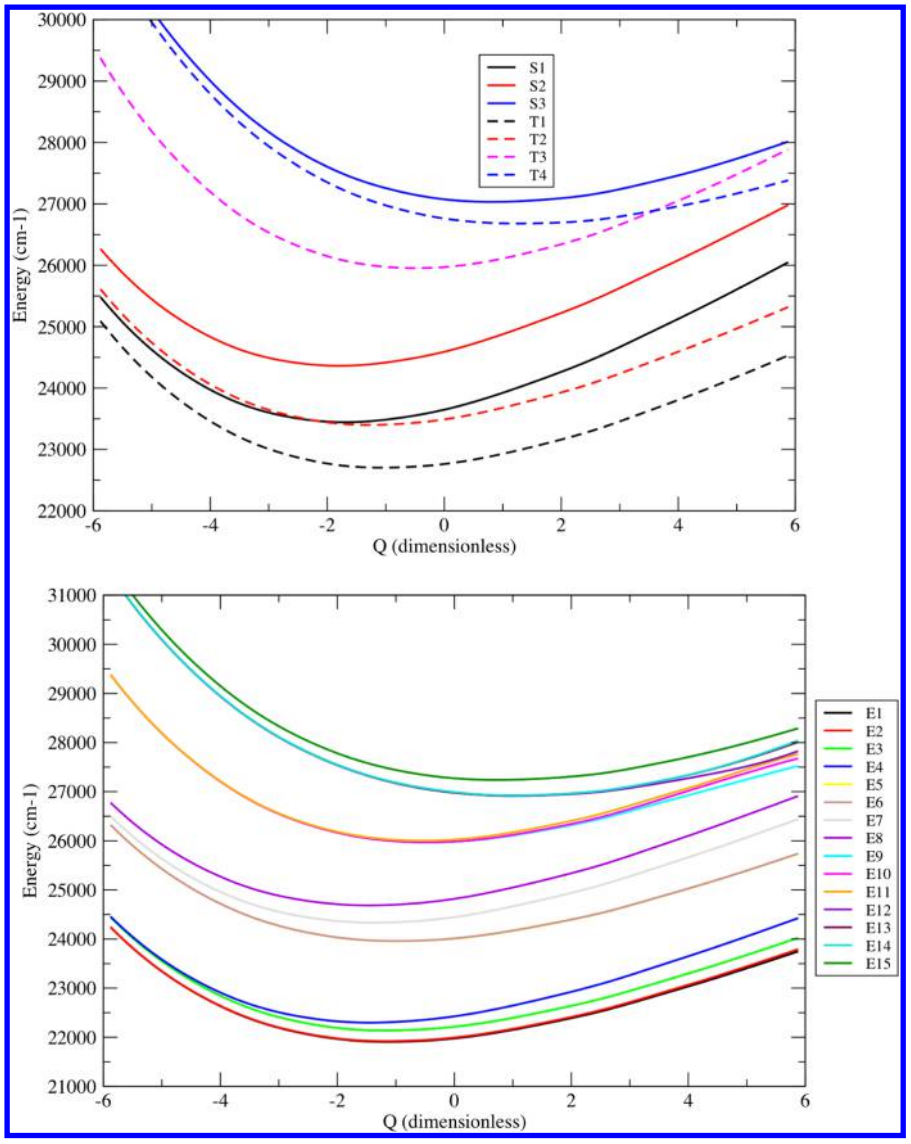

Figure 4. Potential energy curves associated with the low-lying excited states of $[Re(Br)(CO)_3(bpy)]$ **2** calculated without SOC (top) and with SOC (bottom) as a function of the mass and frequency weighted Re−X stretching mode displacement from Franck−Condon ($Q = 0$) (in CH_3CN).

The S_1/T_2, S_2/T_1, and T_1/T_2 SOC evolve similarly in the three complexes along the Q coordinate as shown in Figure 5, Supporting Information Figures S5 and S6 but with larger real-SOC values for the iodide complex **3** greater than 1000 cm^{-1} (Supporting Information Figure S6 top). We may notice in the iodide complex **3** an important variation of S_2/T_3 and S_1/T_4 real-SOC and S_1/T_4 imaginary-SOC that increase drastically with the Re−I bond distance. The significant enhancement of S_2/T_3 real-SOC from 350 to 900 cm^{-1} in $[Re(I)(CO)_3(bpy)]$ (Supporting Information Figure S6 (top)) as a function of the Re−X stretching mode displacement (Q), points to the importance of vibronic spin−orbit coupling immediately after absorption at the early stage of the photophysical process. Indeed, while the predominant XLCT character in the iodide substituted complex (see Figure 2) weakens the SOC effects it enhances the involvement of the Re−I vibrational mode in the vibronic spin−orbit coupling.

Obviously, the SOC behavior along other nuclear coordinates and other nuclear deformations around Franck−Condon has to be investigated to fully understand the mechanism of ultrafast luminescence decay in the title complexes. Moreover, calculated spin−orbit data could certainly be improved by more accurate relativistic calculations, especially for $[Re(I)(CO)_3(bpy)]$ that combines two heavy atoms. Exploratory wavepacket propagations on the spin−orbit coupled PEC described above are discussed in the next section.

3.5. Wavepacket Propagations. The evolution, as a function of time, of the populations of the low-lying S_1, T_1, T_2, and T_3 excited states after absorption to S_2 has been obtained by wavepacket propagations on the "spin-free" PEC (Figure 4 (top), Supporting Information Figures S3 (top) and S4 (top)). The variation of the SOC as a function of the Re−X stretching mode (Figure 5, Supporting Information Figures S5 and S6) has been taken into account in this preliminary one-dimensional simulation. Figure 6 shows the evolution of population in $[Re(Br)(CO)_3(bpy)]$ within the first 500 fs, whereas Supporting Information Figures S7, S8, and S9 exhibit the evolution of population in $[Re(Cl)(CO)_3(bpy)]$, $[Re(Br)(CO)_3(bpy)]$, and $[Re(I)(CO)_3(bpy)]$, respectively, within the first ps.

At the early stage SOC controls the ultrafast population of T_1 that exceeds 20% within 10 fs as illustrated in Figure 6 for

dx.doi.org/10.1021/ct500846n | J. Chem. Theory Comput. 2015, 11, 99−110

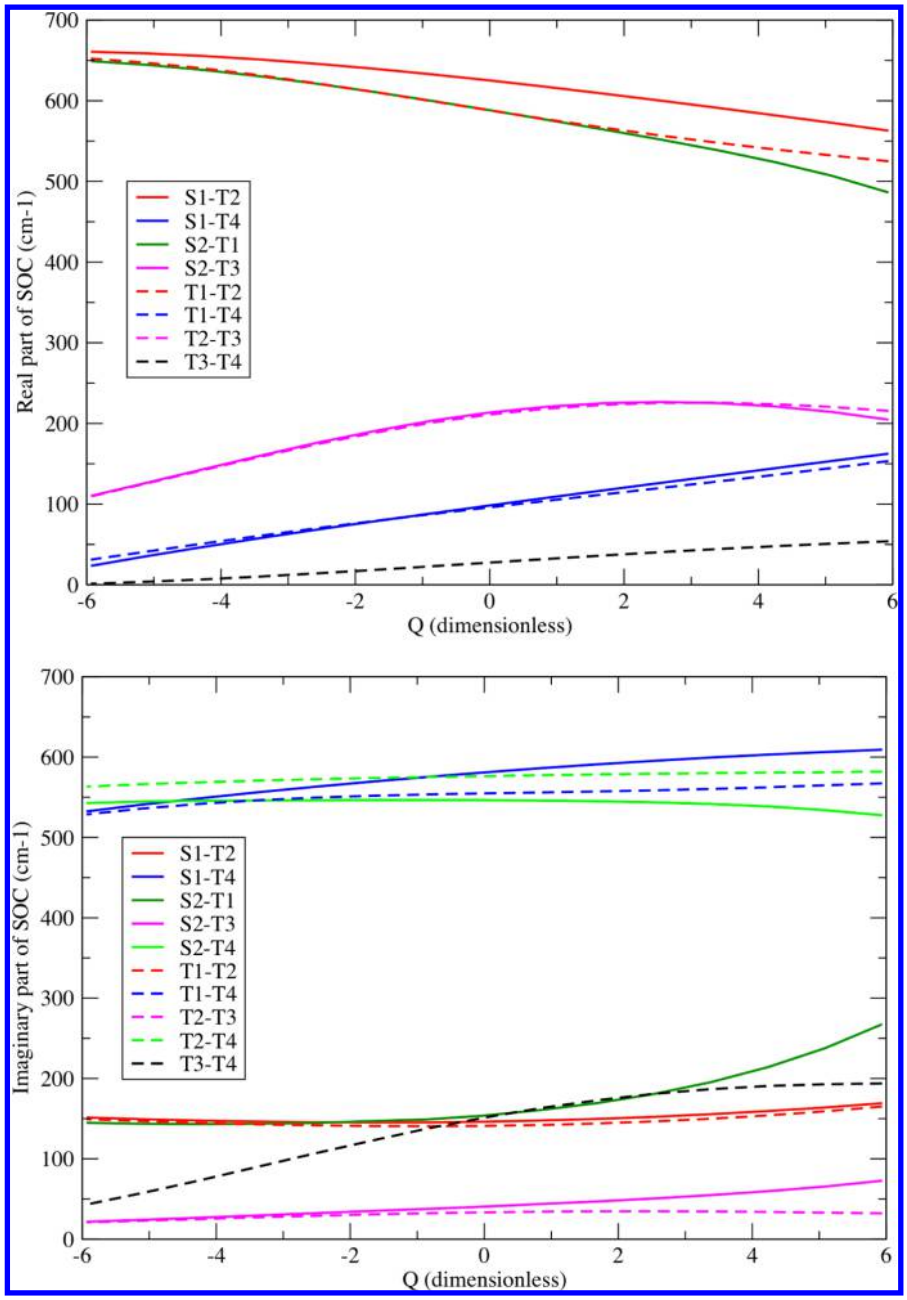

Figure 5. Variation of the SOC matrix elements between the S_1, S_2, S_3, T_1, T_2, T_3, and T_4 electronic states of $[Re(Br)(CO)_3(bpy)]$ **2** calculated as a function of the mass and frequency weighted Re−X stretching mode displacement from Franck−Condon ($Q = 0$) (in CH_3CN): absolute values of real contributions (top); absolute values of imaginary contributions (bottom).

$[Re(Br)(CO)_3(bpy)]$. This is a consequence of the large SOC between S_2 (A′) and the two A′ components of T_1. The two A′ components of T_3 are populated as well but less efficiently (<10%) because of the moderate SOC with S_2. The direct $S_2 \rightarrow S_1$ transition is forbidden by symmetry and the probability of $S_2 \rightarrow T_2$ transition that involves the same orbitals excitation is low. However, at longer time-scales, as soon as T_1 and T_3 are populated, T_2 coupled to T_1 and T_3 by SOC (Figure 5) is potentially populated as long as symmetry rules are respected at the spin−orbit sublevels (Table 4). Indeed the A′ component of T_2 is marginally populated (<0.2%) within the first 25 fs by SOC with the A′ components of T_1 and T_3.

After 1 ps the total populations of S_2, T_1 and T_3 remain nearly constant with average values of 67%, 24%, and 9%, respectively (Supporting Information Figure S8). It should be pointed out that the ISC process simulated here via the $S_2 \rightarrow T_1$, T_3 and T_1,$T_3 \rightarrow T_2$ transitions excludes the A″ pathways that will be activated only by vibronic spin−orbit coupling along a″ normal modes.

At short time-scale $[Re(Cl)(CO)_3(bpy)]$ behaves similarly to $[Re(Br)(CO)_3(bpy)]$ showing an ultrafast population of T_1 (<20%) within less than 10 fs and population of T_3 (<10%) within 20 fs and a negligible population of T_2. Due to smaller values of SOC the ISC is less efficient in the chloride substituted complex with average populations of S_2, T_1, and T_3 of 74%, 16%, and 10%, respectively, within 1 ps (Supporting Information Figure S7).

The population exchange between S_2 and T_1 is more dramatic in $[Re(I)(CO)_3(bpy)]$ due to large SOC (>1000 cm^{-1}) with an ultrafast population of T_1 within 10 fs (40%)

dx.doi.org/10.1021/ct500846n | J. Chem. Theory Comput. 2015, 11, 99−110

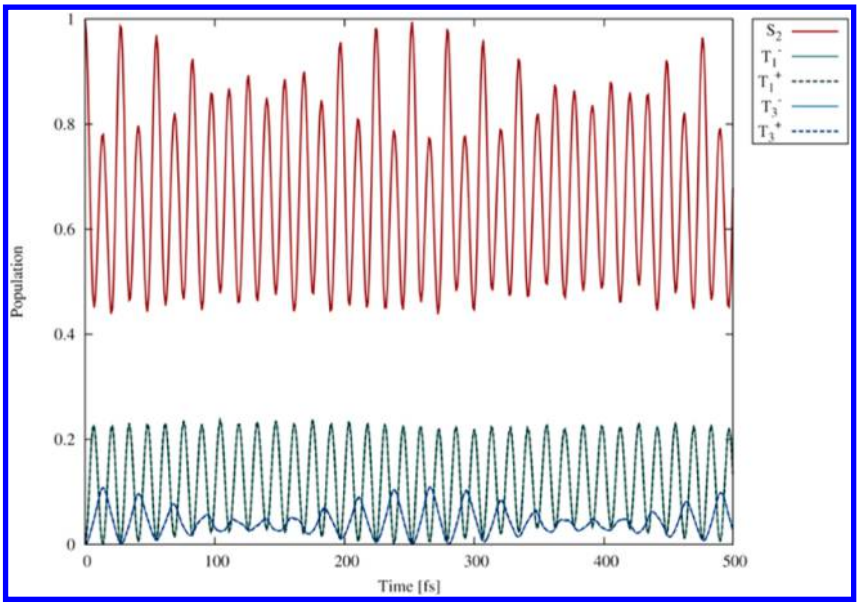

Figure 6. Time-evolution of the population of S_2, T_1, and T_3 excited states of [Re(Br)$(CO)_3$(bpy)] within 500 fs. The population of the A′ spin−orbit sublevels of T_1 and T_3 is represented.

(Supporting Information Figure S9). The population of T_3 reaches nearly 20% in the first 20 fs. The population of T_2 remains marginal, and the average populations of S_2, T_1, and T_3 amount to 46%, 41%, and 13%, respectively.

Whereas the heavy atom effect does not impact the time scale of ISC within the first picaseconds, it does influence significantly the ratio of population of the triplet states.

CONCLUSION

The first complete quantum chemical study of the electronic, structural, and emissive properties of a series of halide substituted Re(I) carbonyls α-diimine complexes investigated experimentally has enabled us to propose a qualitative mechanism for the ultrafast luminescent decay through the seven low-lying singlet and triplet excited states coupled by SOC in acetonitrile. According to our previous studies based on SOC multistate complete active space perturbation theory second order (MS-CASPT2),[14] we have shown that TD-DFT within the ZORA approximation provides realistic absorption spectra and allows the interpretation of the emissive properties of this class of molecules on a semiquantitative static basis. At least six excited states, two singlets and four triplets, are involved in the ISC processes underlying the ultrafast decay after absorption at 400 nm. In contrast to the iodide complex and in a first approximation, the time-resolved luminescence spectra of [Re(Cl)$(CO)_3$(bpy] and [Re(Br)$(CO)_3$(bpy] can be analyzed on the basis of the emission wavelengths calculated without SOC correction. Whereas the S_2 absorbing state is responsible for the initial signal of luminescence characterized by an ultrafast decay of a few tens of fs, the intermediate signal between 500 and 600 nm with a decay of a few hundreds of fs is attributed to both S_1 and T_2 in these two complexes. The long-lived emission at 600−610 nm originates into the deactivation of the lowest T_1 state. [Re(I)$(CO)_3$(bpy] behaves differently because spin−orbit splitting of the triplet states and singlet/triplet mixing becomes important and cannot be ignored. Consequently the luminescence decay should be interpreted on the basis of the spin−orbit sublevels of the original singlet's and triplets. Three domains of energy may be distinguished for the iodide complex: (i) the lowest one involving three nearly degenerate A′ spin−orbit states issue from T_1 and T_2 calculated at 610−620 nm and responsible for the long-lived emission; (ii) a second one involving the spin−orbit states of S_1 (A″) and S_2 (A′) at 577−595 nm controlling the intermediate time scale of 1 ps; (iii) a third one corresponding to the A′ spin−orbit sublevel of T_3 calculated at 512 nm responsible for the early ultrafast decay of 152 fs together with S_2.

In order to investigate the nuclear deformation at Franck−Condon and to infer the interplay between SOC and nuclear relaxation for a subsequent quantum dynamical study, we have calculated the PEC (without and with SOC) and the SOC evolution of the seven lowest singlet and triplet excited states as a function of the mass and frequency weighted Re−X stretching mode displacements. Whereas the PEC are smooth, run in parallel, and very similar for [Re(Cl)$(CO)_3$(bpy] and [Re(Br)-$(CO)_3$(bpy], the shapes of the potentials are more complicated for the iodide complex with a number of avoided crossings appearing at long Re−I bond distances. This is correlated to the strong influence of the SOC that generates important mixing between states. Moreover, some SOC values, especially between the S_2 absorbing state and T_3 increase dramatically with the Re−I stretching mode pointing to a non-negligible interplay between vibronic and spin−orbit couplings.

The accuracy of the spin−orbit data, namely the singlet/triplet coupling and the triplet splitting in [Re(I)$(CO)_3$(bpy)] **3** could certainly be improved by better relativistic calculations going beyond the current level of zero-order approximation. This will be the subject of an ongoing study. The luminescence theoretical data reported in the present work have been obtained under the C_s symmetry constraint. Broken symmetry solutions, the validity of which is always uncertain within the framework of DFT especially for excited states geometry optimization, could lead to slightly different values but probably not to a different interpretation.

Exploratory wavepacket propagations on spin−orbit coupled PEC have been able to simulate partly the ultrafast ISC process observed experimentally via the A′ channels. This preliminary

dx.doi.org/10.1021/ct500846n | J. Chem. Theory Comput. 2015, 11, 99−110

one-dimensional simulation has shown the importance of vibronic spin−orbit coupling in transition metal complexes.

■ ASSOCIATED CONTENT

Supporting Information

Nuclear coordinates of the optimized structures, theoretical electronic densities and absorption spectra, potential energy and SOC curves for complexes **1** and **3**. Time evolution of the excited state's population in complexes **1** and **3**. This material is available free of charge via the Internet at http://pubs.acs.org.

■ AUTHOR INFORMATION

Corresponding Author

*E-mail: c.daniel@unistra.fr.

Notes

The authors declare no competing financial interest.

■ ACKNOWLEDGMENTS

The authors thank A. Vlček, Jr., M. Chergui, and A. Cannizzo for having motivated this work. We are grateful to S. Záliš for fruitful discussions. The European actions COST perspect-H_2O and CODEC are acknowledged. The quantum chemical calculations have been performed on the computer nodes of the LCQS, Strasbourg, and the authors thank the computer facilities of the High Performance Computing regional center of Unistra.

■ REFERENCES

(1) Juban, E. A.; Smeigh, A. L.; Monat, J. E.; McCusker, J. K. *Coord. Chem. Rev.* **2006**, *250*, 1783.
(2) McCusker, J. K. *Acc. Chem. Res.* **2003**, *36*, 876.
(3) Chergui, M. *Dalton Trans.* **2012**, *41*, 13022.
(4) Bräm, O.; Messina, F.; Baranoff, E.; Cannizzo, A.; Nazeeruddin, M. K.; Chergui, M. *J. Phys. Chem. C* **2013**, *117*, 15958.
(5) El Nahhas, A.; Consani, C.; Blanco-Rodríguez, A. M.; Lancaster, K. M.; Bräm, O.; Cannizzo, A.; Towrie, M.; Clark, I. P.; Záliš, S.; Chergui, M.; Vlček, A., Jr. *Inorg. Chem.* **2011**, *50*, 2932.
(6) Renske, M.; van der Veen, R. M.; Cannizzo, A.; van Mourik, F.; Vlček, A., Jr.; Chergui, M. *J. Am. Chem. Soc.* **2011**, *133*, 305.
(7) El Nahhas, A.; Cannizzo, A.; van Mourik, F.; Blanco-Rodríguez, A. B.; Záliš, S.; Vlček, A., Jr.; Chergui, M. *J. Phys. Chem. A* **2010**, *114*, 6361.
(8) Huse, N.; Kim, T. K.; Jamula, L.; McCusker, J. K.; de Groot, F. M. F.; Schoenlein, R. W. *J. Am. Chem. Soc.* **2010**, *132*, 6809.
(9) Huse, N.; Cho, H.; Hong, K.; Jamula, L.; de Groot, F. M. F.; Kim, T. K.; McCusker, J. K.; Schoenlein, R. W. *J. Phys. Chem. Lett.* **2011**, *2*, 880.
(10) Bressler, Ch.; Milne, C.; Pham, V.-T.; El Nahhas, A.; van der Veen, R. M.; Gawelda, W.; Johnson, S.; Beaud, P.; Grolimund, D.; Kaiser, M.; Borca, C. N.; Ingold, G.; Abela, R.; Chergui, M. *Science* **2009**, *323*, 489.
(11) Blanco-Rodríguez, A. M.; Kvapilová, H.; Sýkora, J.; Towrie, M.; Nervi, C.; Volpi, G.; Záliš, S.; Vlček, A., Jr. *J. Am. Chem. Soc.* **2014**, *136*, 5963.
(12) Visscher, L.; Saue, T.; Nieuwpoort, W. C.; Faegri, K.; Gropen, O. *J. Chem. Phys.* **1993**, *99*, 6704.
(13) Vallet, V.; Strich, A.; Daniel, C. *Chem. Phys.* **2005**, *13*, 18.
(14) Heydová, R.; Gindensperger, E.; Romano, R.; Sýkora, J.; Vlček, A., Jr.; Záliš, S.; Daniel, C. *J. Phys. Chem. A* **2012**, *116*, 11319−11329.
(15) Heitz, M. C.; Ribbing, C.; Daniel, C. *J. Chem. Phys.* **1997**, *106*, 1421.
(16) Guillaumont, D.; Daniel, C. *J. Am. Chem. Soc.* **1999**, *121*, 11733.
(17) Bruand-Cote, I.; Daniel, C. *Chem. Eur. J.* **2002**, *8*, 1361.
(18) Daniel, C.; Guillaumont, D.; Ribbing, C.; Minaev, B. *J. Phys. Chem. A* **1999**, *103*, 5766.
(19) Minaev, B.; Baryshnikov, G.; Ågren, H. *Phys. Chem. Chem. Phys.* **2014**, *16*, 1719.
(20) Daniel, C. *Coord. Chem. Rev.* **2015**, *282*−*283*, 19.
(21) Li, X.; Minaev, B.; Ågren, H.; Tian, H. *J. Phys. Chem. C* **2011**, *115*, 20724.
(22) Brahim, H.; Daniel, C. *Comp. Theor. Chem.* **2014**, *1040*−*1041*, 219.
(23) Papai, M.; Vanko, G.; de Graaf, C.; Rozgonyi, T. *J. Chem. Theory Comp.* **2013**, *9*, 509.
(24) Sousa, C.; de Graaf, C.; Rudavskyi, A.; Broer, R.; Tatchen, J.; Etinski, M.; Marian, C. M. *Chem. Eur. J.* **2013**, *19*, 17541.
(25) Etinski, M.; Tatchen, J.; Marian, C. M. *J. Chem. Phys.* **2011**, *134*, 154105.
(26) Etinski, M.; Rai-Constapel, V.; Marian, C. M. *J. Chem. Phys.* **2014**, *140*, 114104.
(27) Tavernelli, I.; Curchod, B. F. E.; Rothlisberger, U. *Chem. Phys.* **2011**, *391*, 101.
(28) Mondal, P.; Opalka, D.; Poluyanov, L. V.; Domcke, W. *Chem. Phys.* **2011**, *387*, 56.
(29) Mondal, P.; Opalka, D.; Poluyanov, L. V.; Domcke, W. *J. Chem. Phys.* **2012**, *136*, 084308.
(30) Cannizzo, A.; Blanco- Rodríguez, A. M.; El Nahhas, A.; Sebera, J.; Záliš, S.; Vlček, A., Jr.; Chergui, M. *J. Am. Chem. Soc.* **2008**, *130*, 8967.
(31) Becke, A. D. *J. Chem. Phys.* **1993**, *98*, 5648.
(32) Stephens, P. J.; Devlin, F. J.; Chabalowski, C. F.; Frisch, M. J. *J. Phys. Chem.* **1994**, *98*, 11623.
(33) van Lenthe, E.; Baerends, E. J. *J. Comput. Chem.* **2003**, *24*, 1142.
(34) van Lenthe, E.; van Leeuwen, R.; Baerends, E. J.; Snijders, J. G. *Int. J. Quantum Chem.* **1996**, *57*, 281.
(35) Runge, E.; Gross, E. K. U. *Phys. Rev. Lett.* **1984**, *52*, 997.
(36) Petersilka, M.; Gossmann, U. J.; Gross, E. K. U. *Phys. Rev. Lett.* **1996**, *76*, 1212.
(37) Klamt, A.; Schüürmann, G. J. *Chem. Soc., Perkin Trans.* **1993**, *2*, 799.
(38) Klamt, A. *J. Phys. Chem.* **1995**, *99*, 2224.
(39) Klamt, A.; Jones, V. J. *Chem. Phys.* **1996**, *105*, 9972.
(40) Rosa, A.; Baerends, E. J.; van Gisbergen, S. J. A.; van Lenthe, E.; Groeneveld, J. A.; Snijders, J. G. *J. Am. Chem. Soc.* **1999**, *121*, 10356.
(41) Pye, C.; Ziegler, T. *Theor. Chem. Acc.* **1999**, *101*, 396.
(42) Meyer, H.-D.; Manthe, U.; Cederbaum, L. S. *Chem. Phys. Lett.* **1990**, *165*, 73.
(43) Beck, M. H.; Jägle, A.; Worth, G. A.; Meyer, H.-D. *Phys. Rep.* **2000**, *324*, 1.
(44) *Multidimensional Quantum Dynamics MCTDH Theory and Applications*; Meyer, H.-D., Gatti, F., Worth, G. A., Eds.; Wiley-VCH: Weinheim, 2009.
(45) *ADF, SCM, Theoretical Chemistry*; Vrije Universiteit: Amsterdam, The Netherlands, 2013; https://www.scm.com/Downloads/2013.
(46) Kohout, M. *DGrid*, version 4.5; Springer: Radebeul, 2009.
(47) Capano, G.; Penfold, T. J.; Röthlisberger, U.; Tavernelli, I. *CHIMIA* **2014**, *68*, 227.